Supplementary Material

Self-Assembled of Thioether-Bridged Paclitaxel-dihydroartemisinin prodrug for amplified antitumor efficacy based cancer ferroptotic - chemo therapy

Yifei Zheng [a,1], Chao Qin [a,1], Fei Li[a], Jingxin Qi[a], Xinyu Chu[a], Hao Li[a], Ting Shi[a], Zhen Yan[a], Lei Yang[a], Xiaofei Xin[a], Lisha Liu[a], Xiaopeng Han [a*] and Lifang Yin[a*,b,c]

[a] Department of Pharmaceutics, China Pharmaceutical University, Nanjing 210009, China

[b] NMPA Key Laboratory for Research and Evaluation of Pharmaceutical Preparations and Excipients, China Pharmaceutical University, Nanjing 210009, China

[c] Key Laboratory of Drug Quality Control and Pharmacovigilance, China Pharmaceutical University, China; State Key Laboratory of Natural Medicine, China Pharmaceutical University, Nanjing,210009, China

[1] These authors contributed equally to this article

Corresponding Author

* (Xiaopeng Han) nkhxp15@163.com

*(Lifang Yin) lifangyin_@163.com

Supplementary Figure Captions

Scheme S1. Synthesis of paclitaxel-thiodiglycolic acid-dihydroartemisinin conjugate (PSD).

Scheme S2. Synthesis of the paclitaxel-glutaric acid-dihydroartemisinin conjugate (PCD).

Scheme S3. Synthesis of the Ferrocene-PEG conjugate (Fc).

Figure S1. ^{1}H NMR spectrum of paclitaxel in $CDCl_3$.

Figure S2. ^{1}H NMR spectrum of dihydroartemisinin (DHA) in $CDCl_3$.

Figure S3. ^{1}H NMR spectrum of paclitaxel-thiodiglycolic acid conjugate(PS) in $CDCl_3$.

Figure S4. ^{1}H NMR spectrum of paclitaxel-thiodiglycolic acid-dihydroartemisinin conjugate (PSD) in $CDCl_3$.

Figure S5. ESI/MS spectrum of paclitaxel-thiodiglycolic acid-dihydroartemisinin conjugate (PSD).

Figure S6. ^{1}H NMR spectrum of paclitaxel -glutaric acid-dihydroartemisinin(PCD) in $CDCl_3$.

Figure S7. ESI/MS spectrum of paclitaxel-glutaric acid-dihydroartemisinin (PCD).

Figure S8. ^{1}H NMR spectrum of Ferrocene-PEG conjugate (Fc) in $CDCl_3$.

Figure S9. ROS responsiveness of the conjugate of PSD.

Figure S10. ROS responsiveness of the conjugate of PCD.

Figure S11. The TEM images of nano PSD-Fc and nano PCD-Fc.(bar=500 nm, insert bar=50 nm)

Figure S12. The stability of different nanoparticles in PBS 7.4(A-C) and10% FBS(D-F). (Data are presented as mean ± SD, n = 3)

Figure S13. The TEM images of nano PCD-Fc and nano PSD-Fc after incubation with 10 mM H_2O_2 for 12 h(bar=200 nm).

Figure S14. The high-resolution XPS Fe 2p spectra of nano PSD-Fc.

Figure S15. *In vitro* PTX release profiles of formulations in different conditions. (data are mean±SD , n=3, $^{**}P\leq0.01$, $^{***}P\leq0.001$)

Figure S16. Cellular uptake of different formulations on 4T1 cells at 37 ℃ measured by flow cytometry(A) and the fluorescent intensity of different formulations in 4T1 cells(B) (data are mean±SD, n=3, $^{*}P\leqslant0.05$, $^{**}P\leqslant0.01$, $^{***}P\leqslant0.001$, $^{\#}P\leqslant0.0001$, FITC dosage: 2.0 μg/mL)

Figure S17. Time-dependent intracellular of nano DiO-DiI/PCD, nano DiO-DiI/PSD, and nano DiO-DiI/PSD-Fc in 4T1cells imaged by CLSM.

Figure S18. CLSM and flow cytometry images of the DCFH-DA probe in 4T1 cells after Fc, PTX treatments.

Figure S19. CLSM and flow cytometry images of the DCFH-DA probe in 4T1 cells after DHA, DHA+Fc treatments.

Figure S20. The CLSM image of the ROS generation in 4T1 cells after various treatments using the DCFH-DA probe with or without thiourea (ROS Scavenger),

deferoxamine (DFO, iron chelation).

Figure S21. The flow cytometry analysis of the ROS generation in 4T1 cells after various treatments using the DCFH-DA probe with or without thiourea (ROS Scavenger), deferoxamine (DFO, iron chelation).

Figure S22. Western blot analysis of xCT and GPX4 after treatment with different formulations for 24h (DHA concentration at 5 μM).

Figure S23. CLSM images of the BODIPY C11 probe in 4T1 cells after various treatments (ROS detection probe, 10 μM).

Figure S24. CLSM images of the BODIPY C11 probe in 4T1 cells after various treatments with or without thiourea (ROS Scavenger), deferoxamine (DFO, iron chelation).

Figure S25. *In vitro* cytotoxicity against 4T1 cell lines after being incubated with different free drug for 24h.(data are mean±SD, n=3, $^{*}P\leqslant0.05$, $^{**}P\leqslant0.01$, $^{***}P\leqslant0.001$, $^{\#}P\leqslant0.0001$)

Figure S26. *In vitro* cytotoxicity against 4T1, NIH3T3 cell lines after being incubated with different formulations for 24h with or without thiourea (ROS Scavenger), deferoxamine (DFO, iron chelation).(data are mean±SD, n=3, $^{*}P\leqslant0.05$, $^{**}P\leqslant0.01$, $^{\#}P\leqslant0.0001$)

Figure S27. Flow cytometry analysis of cell cycle distribution in 4T1 cells after treatment with different preparations. (data are mean±SD, n=3)

Figure S28. Flow cytometry analysis of apoptosis in 4T1 cells after treatment with different preparations.

Figure S29. *In vivo* fluorescence images of the 4T1 bearing mice after intravenous injection of DiR labeled nanoparticles (A), and Quantitative analysis of relative organ and tumor accumulation at 24 h (B-C). (data are mean ± SD, n=3, $^{\#}P \leqslant 0.0001$)

Figure S30. H&E and TUNEL images of 4T1 xenograft tumors after 14-day treatments(bar=50 μm).

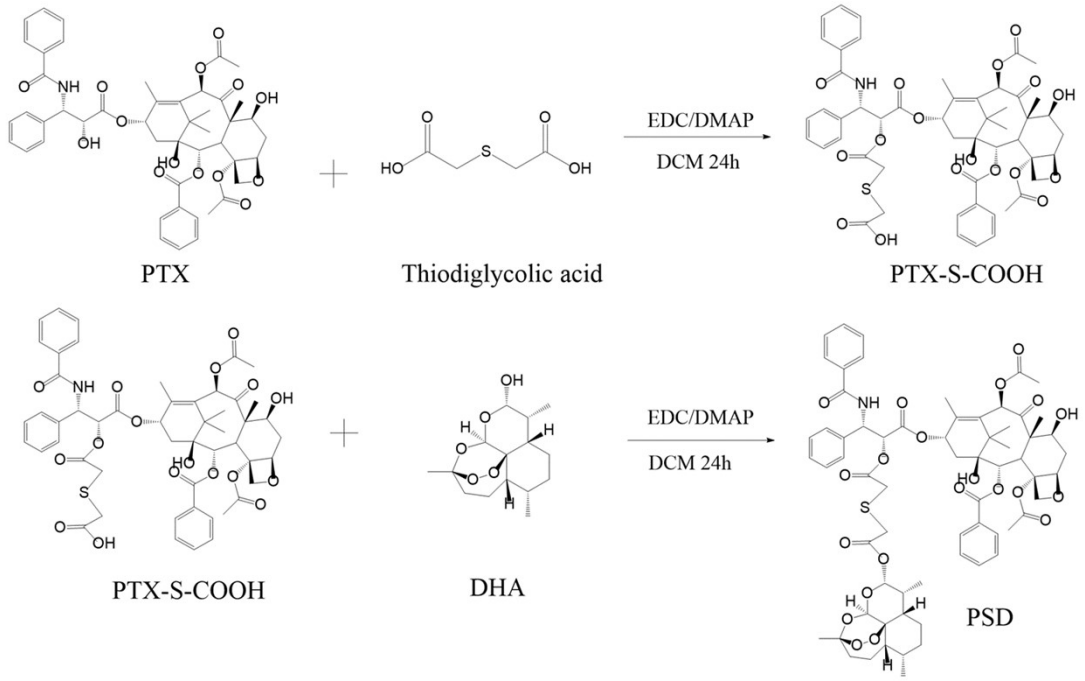

Scheme S1. Synthesis of paclitaxel-thiodiglycolic acid-dihydroartemisinin conjugate (PSD).

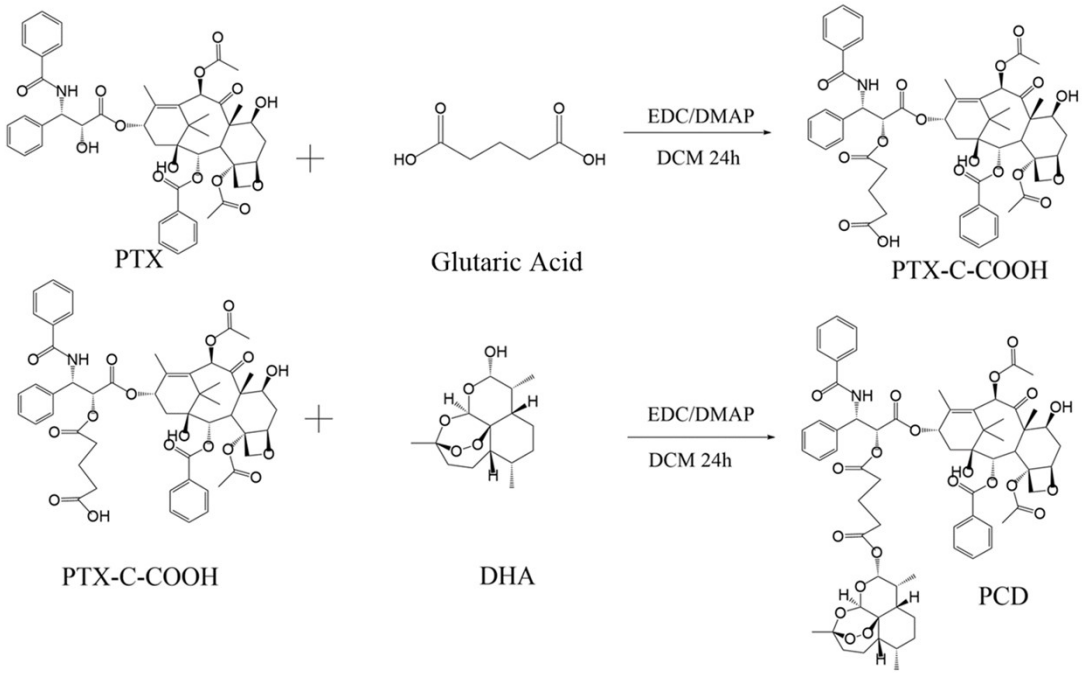

Scheme S2. Synthesis of the paclitaxel-glutaric acid-dihydroartemisinin conjugate (PCD).

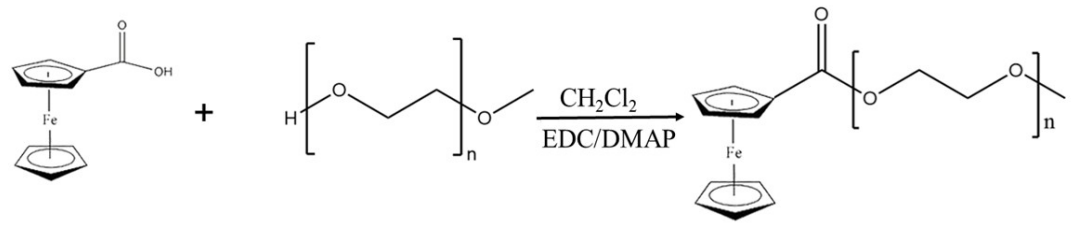

Scheme S3. Synthesis of the Ferrocene-PEG conjugate (Fc).

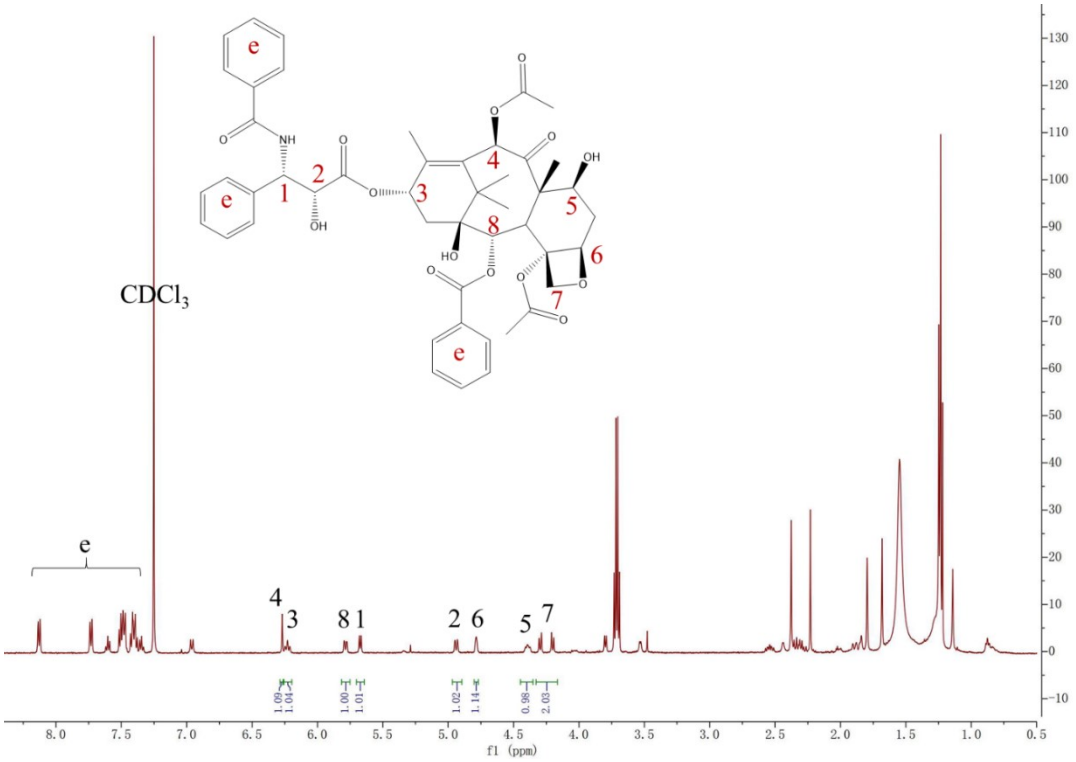

Figure S1. ^{1}H NMR spectrum of paclitaxel in $CDCl_3$.

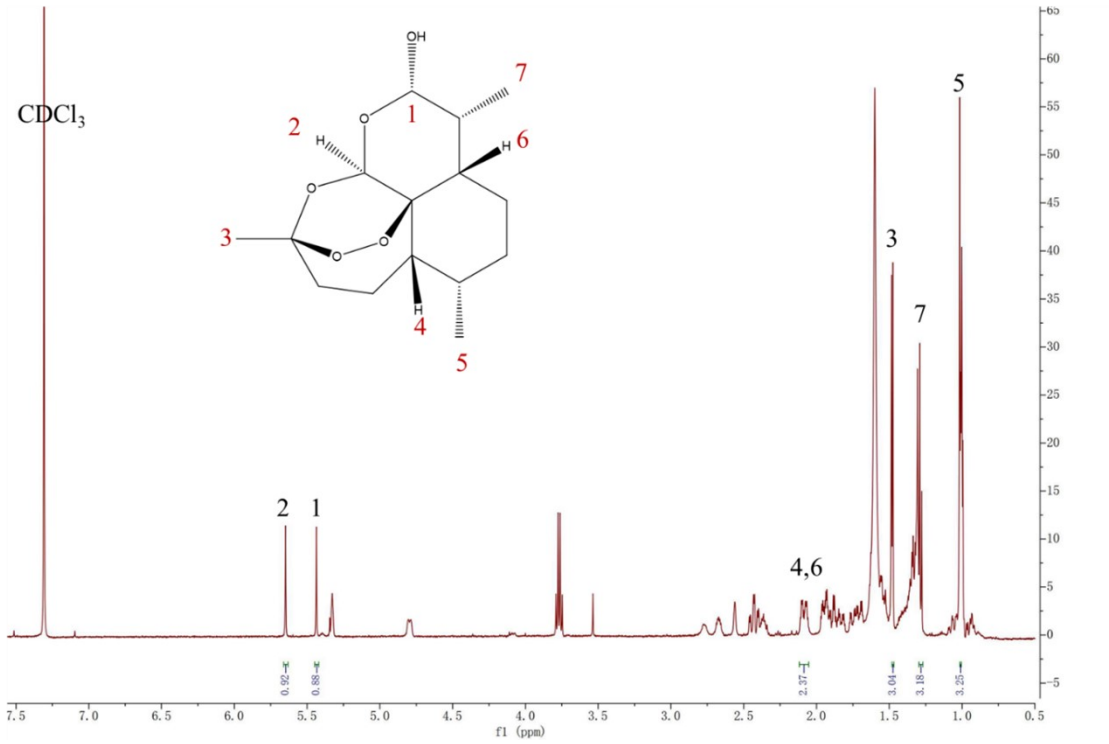

Figure S2. ^{1}H NMR spectrum of dihydroartemisinin (DHA) in $CDCl_3$.

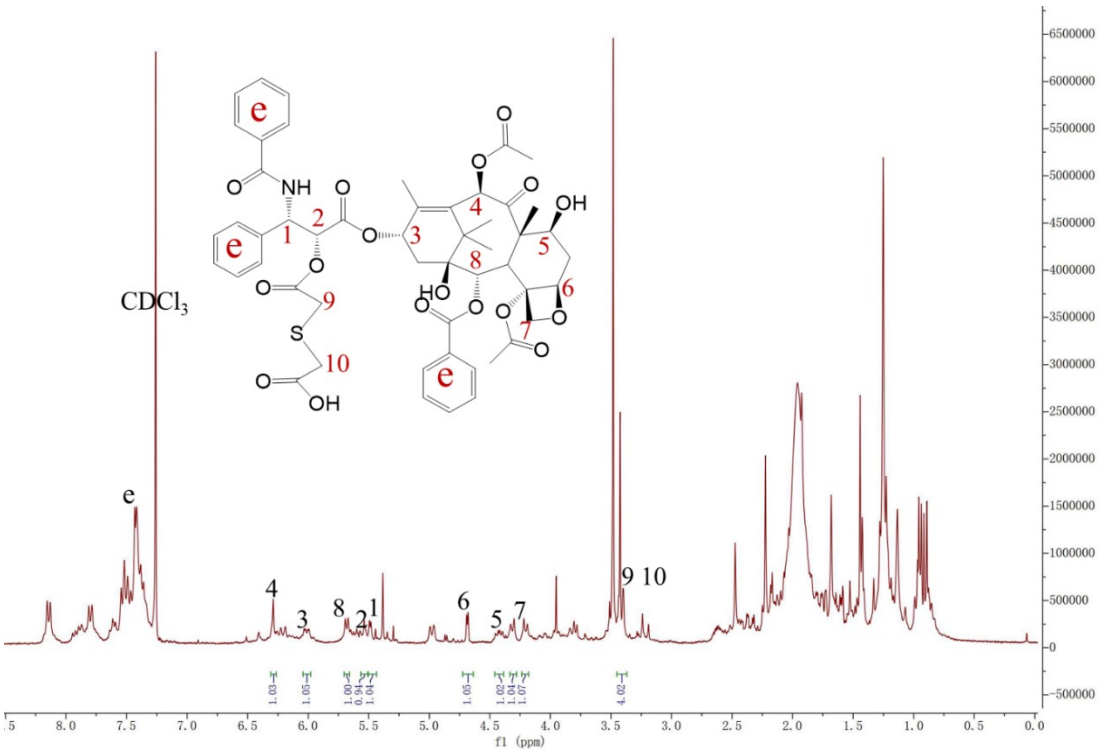

Figure S3. ^{1}H NMR spectrum of paclitaxel-thiodiglycolic acid conjugate (PS) in

$CDCl_3$.

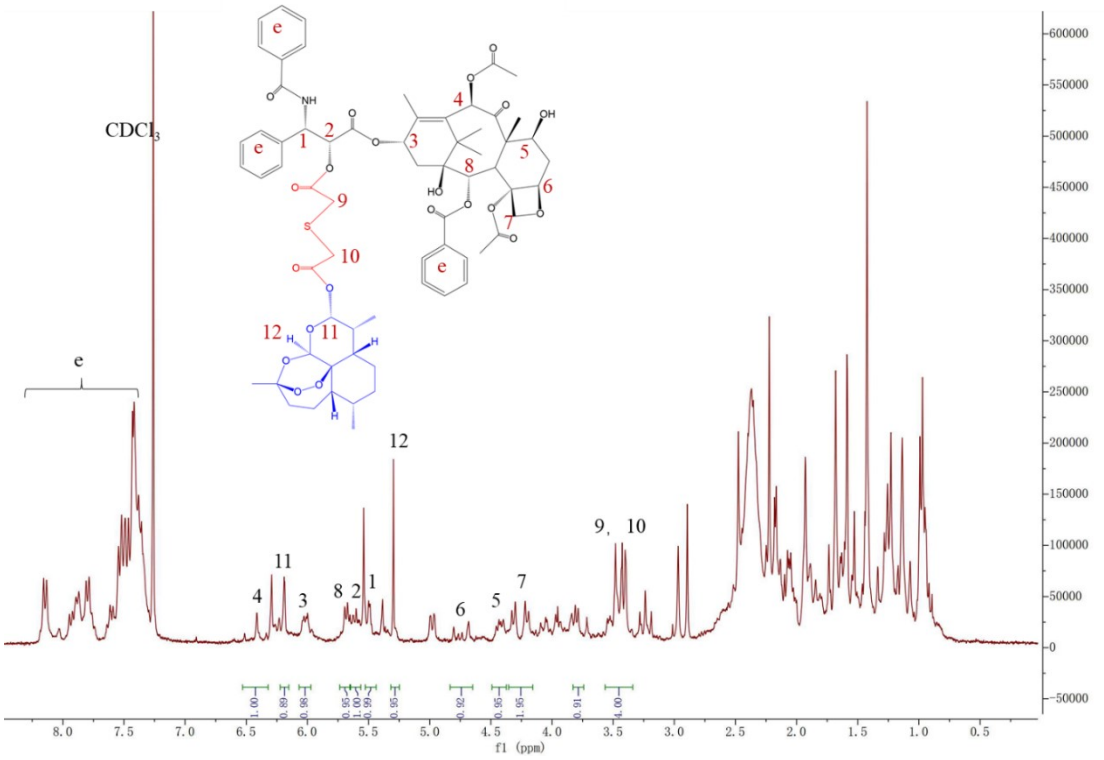

Figure S4. ^{1}H NMR spectrum of paclitaxel-thiodiglycolic acid-dihydroartemisinin conjugate (PSD) in $CDCl_3$.

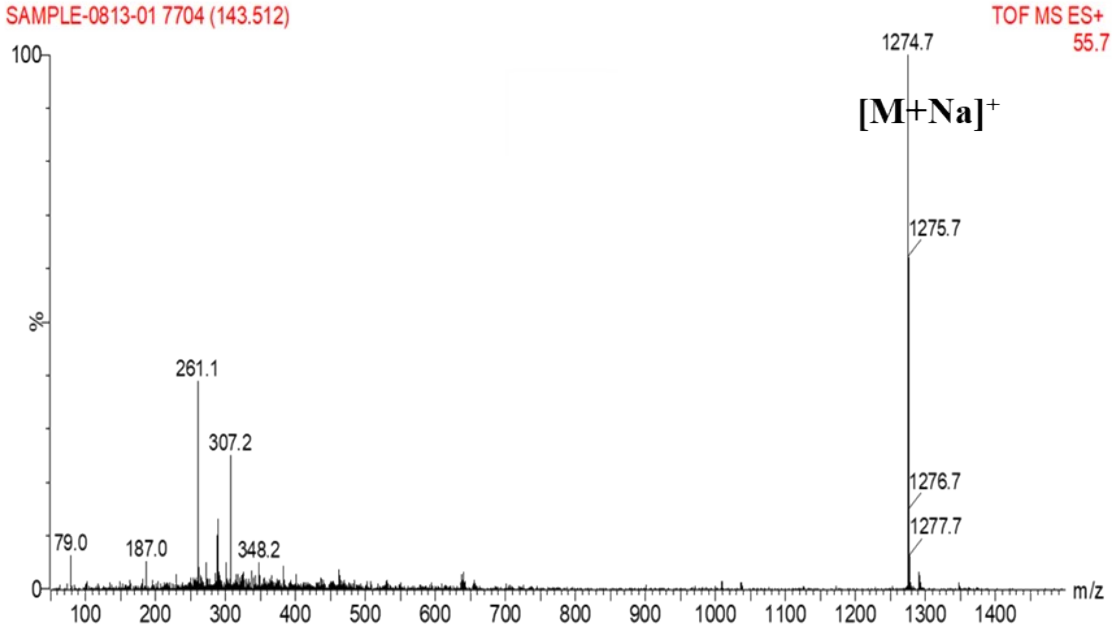

Figure S5. ESI/MS spectrum of paclitaxel-thiodiglycolic acid-dihydroartemisinin conjugate (PSD).

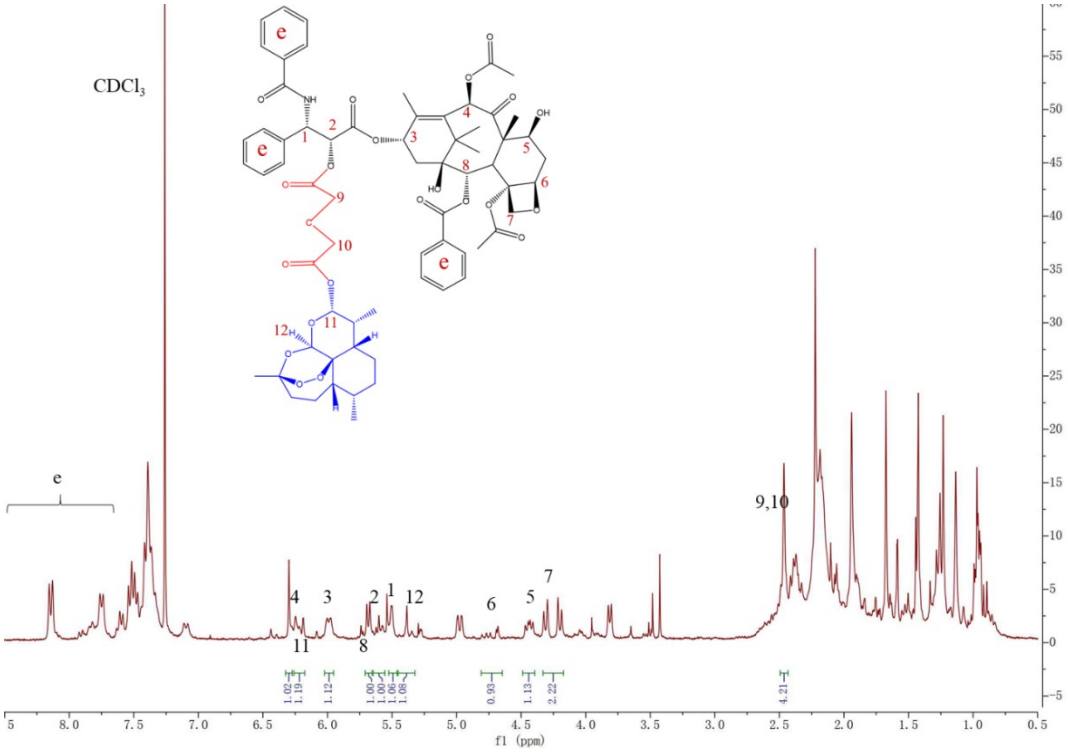

Figure S6. ^{1}H NMR spectrum of paclitaxel -glutaric acid-dihydroartemisinin(PCD) in $CDCl_3$.

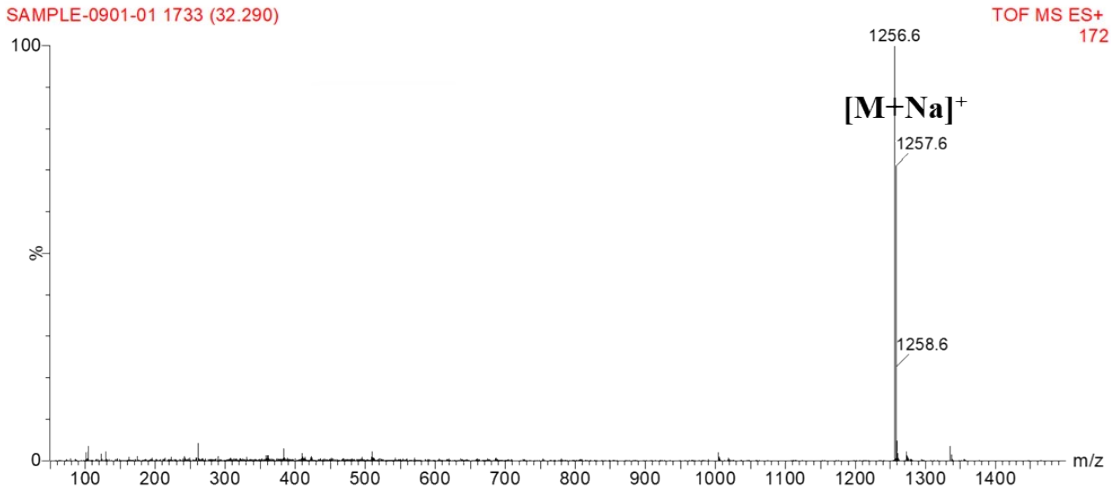

Figure S7. ESI/MS spectrum of paclitaxel-glutaric acid-dihydroartemisinin (PCD).

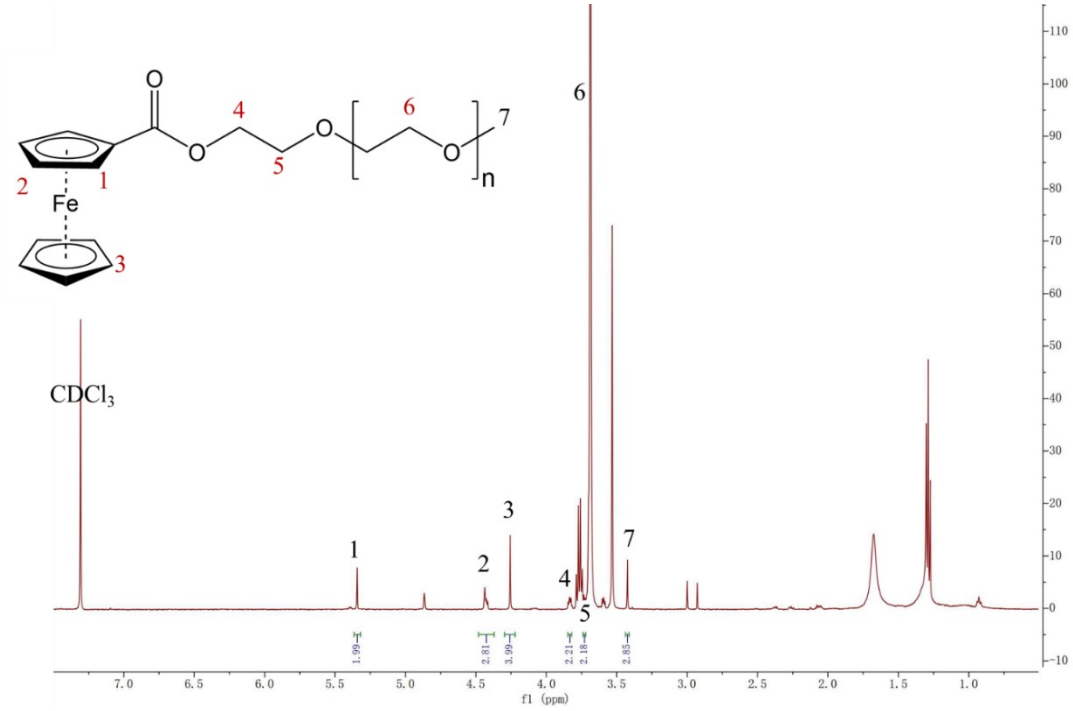

Figure S8. ^{1}H NMR spectrum of Ferrocene-PEG conjugate (Fc) in $CDCl_3$.

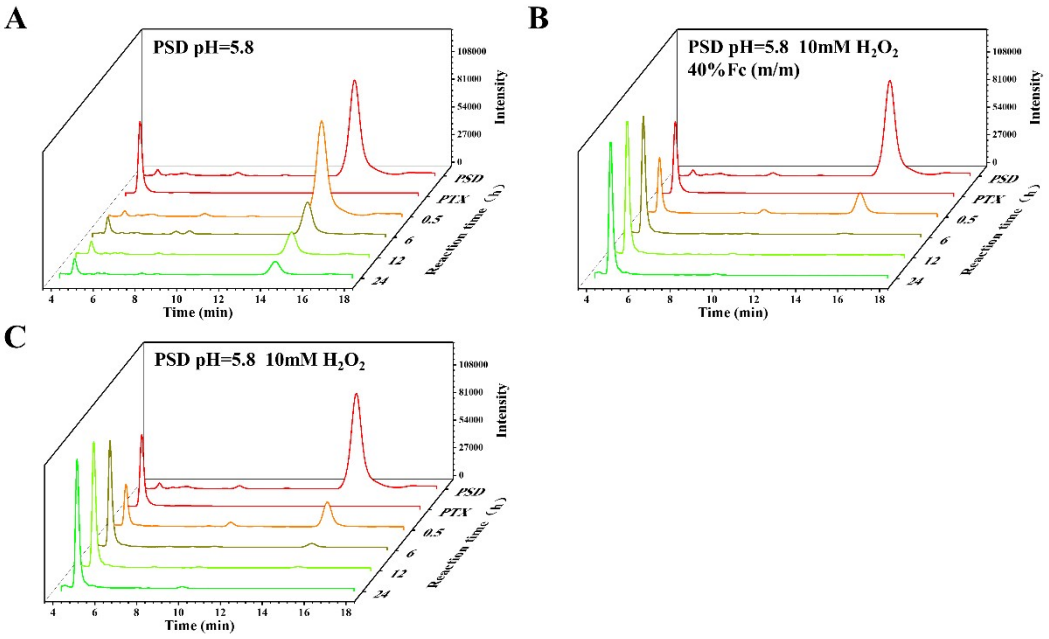

Figure S9. ROS responsiveness of the conjugate of PSD.

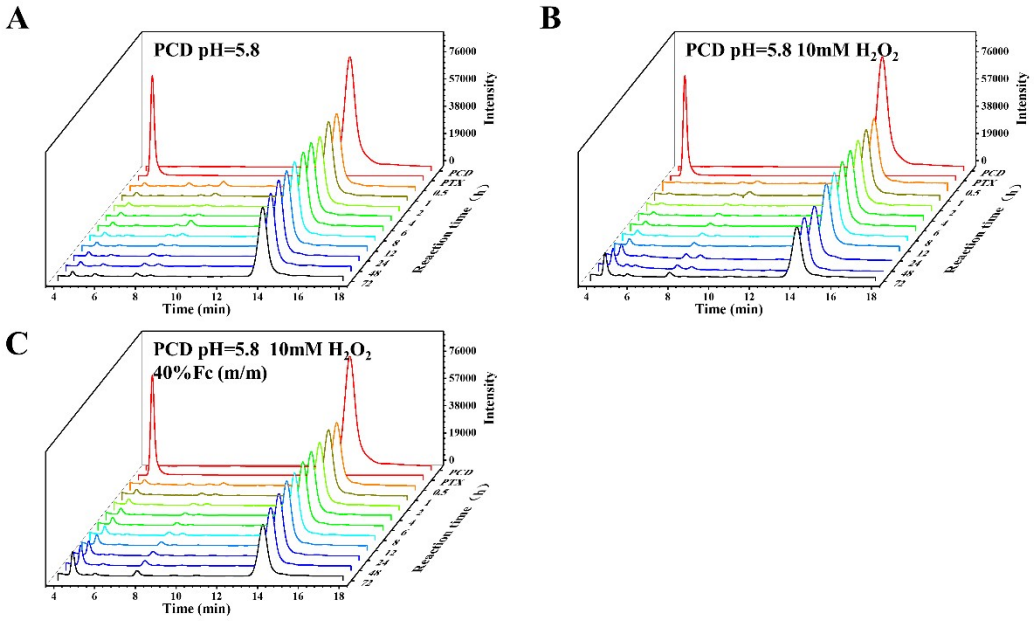

Figure S10. ROS responsiveness of the conjugate of PCD.

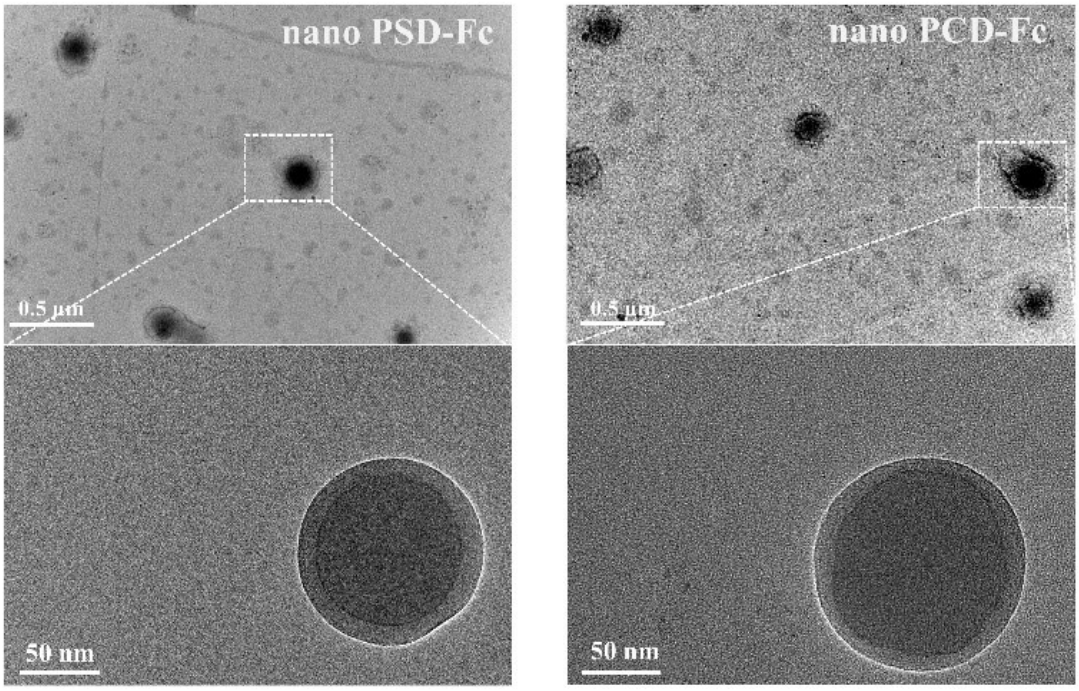

Figure S11. The TEM images of nano PSD-Fc and nano PCD-Fc. (bar=500 nm, insert bar=50 nm)

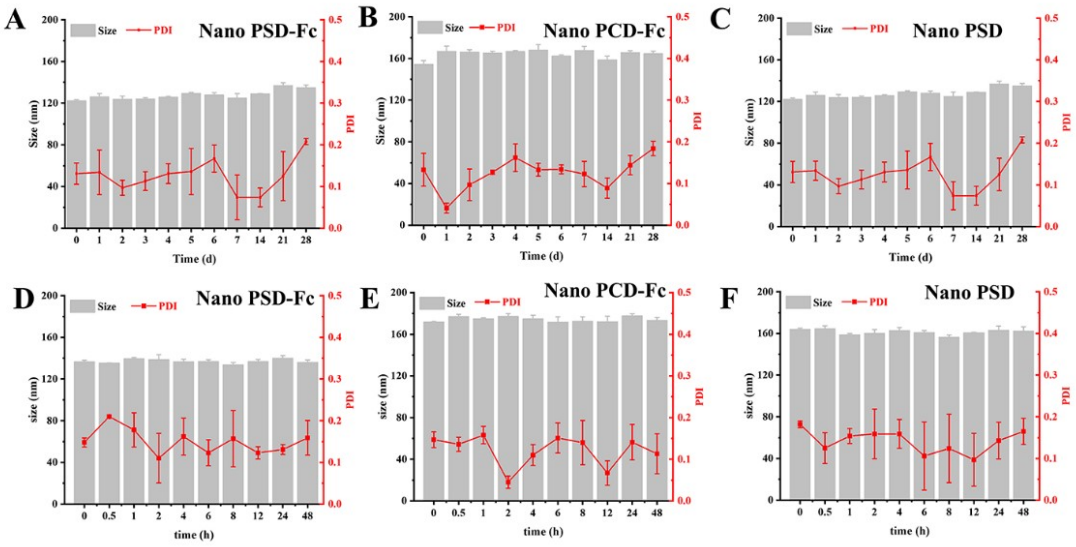

Figure S12. The stability of different nanoparticles in PBS 7.4(A-C) and10% FBS(D-F). (Data are presented as mean ± SD, n = 3)

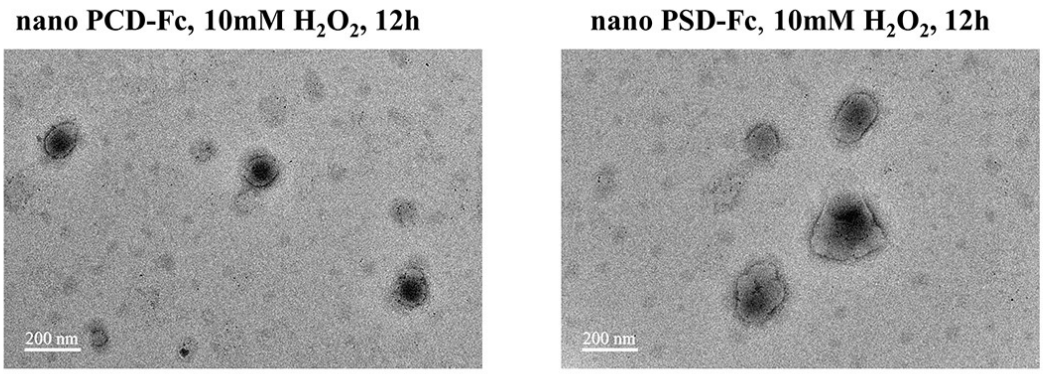

Figure S13. The TEM images of nano PCD-Fc and nano PSD-Fc after incubation with 10 mM H_2O_2 for 12 h(bar=200 nm).

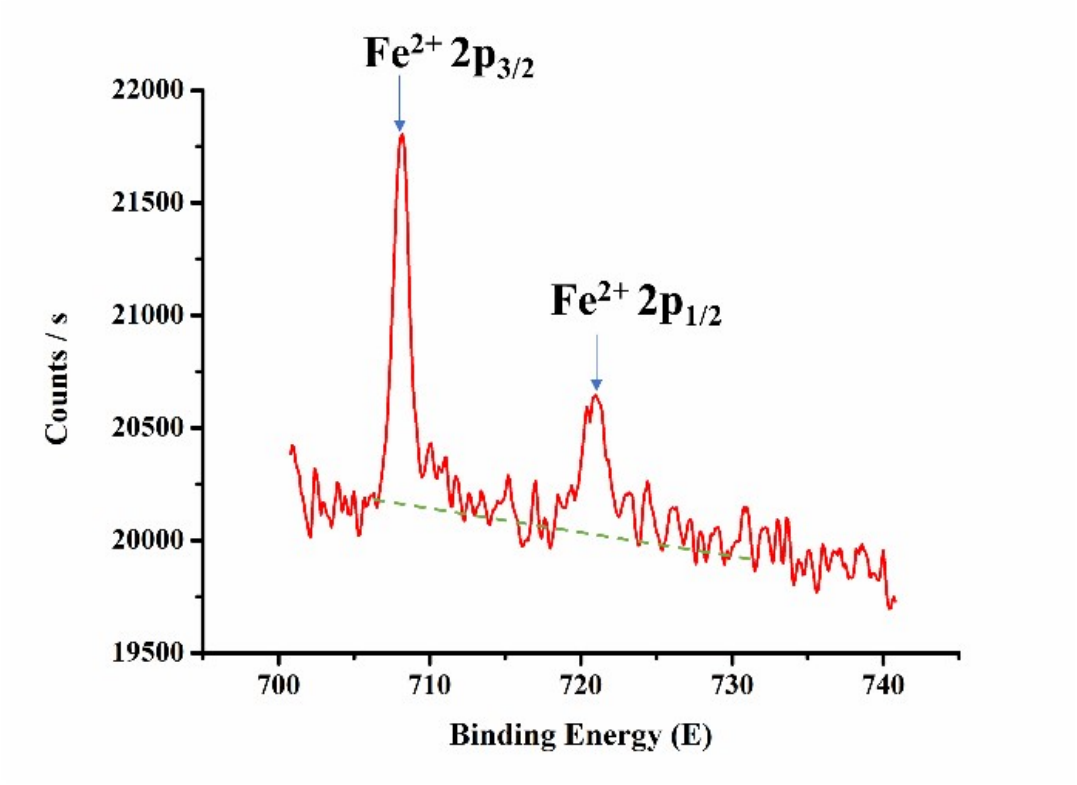

Figure S14. The high-resolution XPS Fe 2p spectra of nano PSD-Fc.

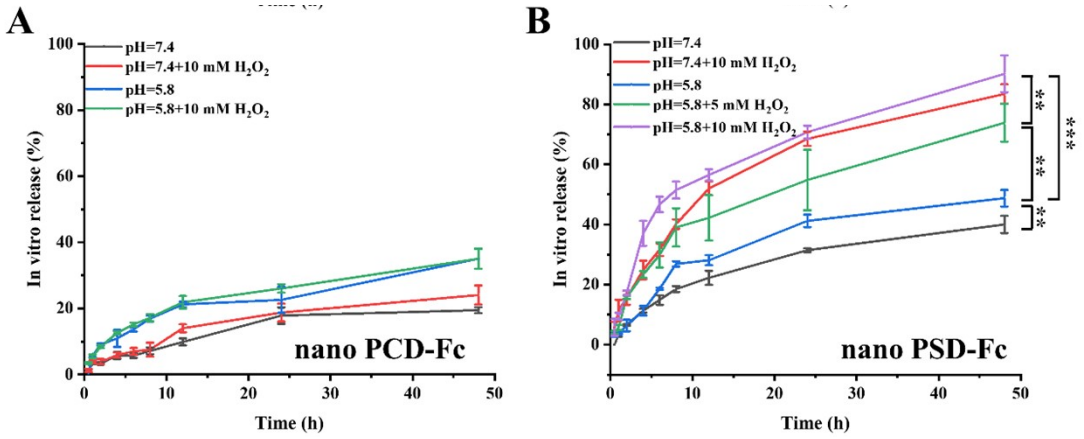

Figure S15. *In vitro* PTX release profiles of formulations in different conditions. (data are mean±SD , n=3, **P≤0.01, ***P≤0.001)

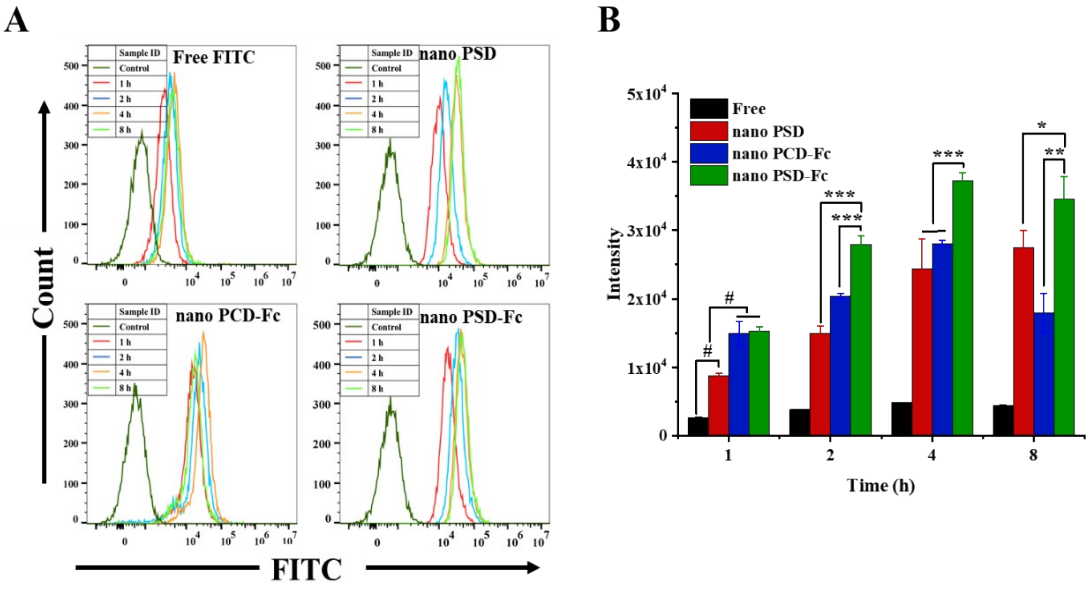

Figure S16. Cellular uptake of different formulations on 4T1 cells at 37 ℃ measured by flow cytometry(A) and the fluorescent intensity of different formulations in 4T1 cells(B) (data are mean±SD, n=3, *P≤0.05 , **P≤0.01, ***P≤0.001, #P≤0.0001, FITC dosage: 2.0 μg/mL)

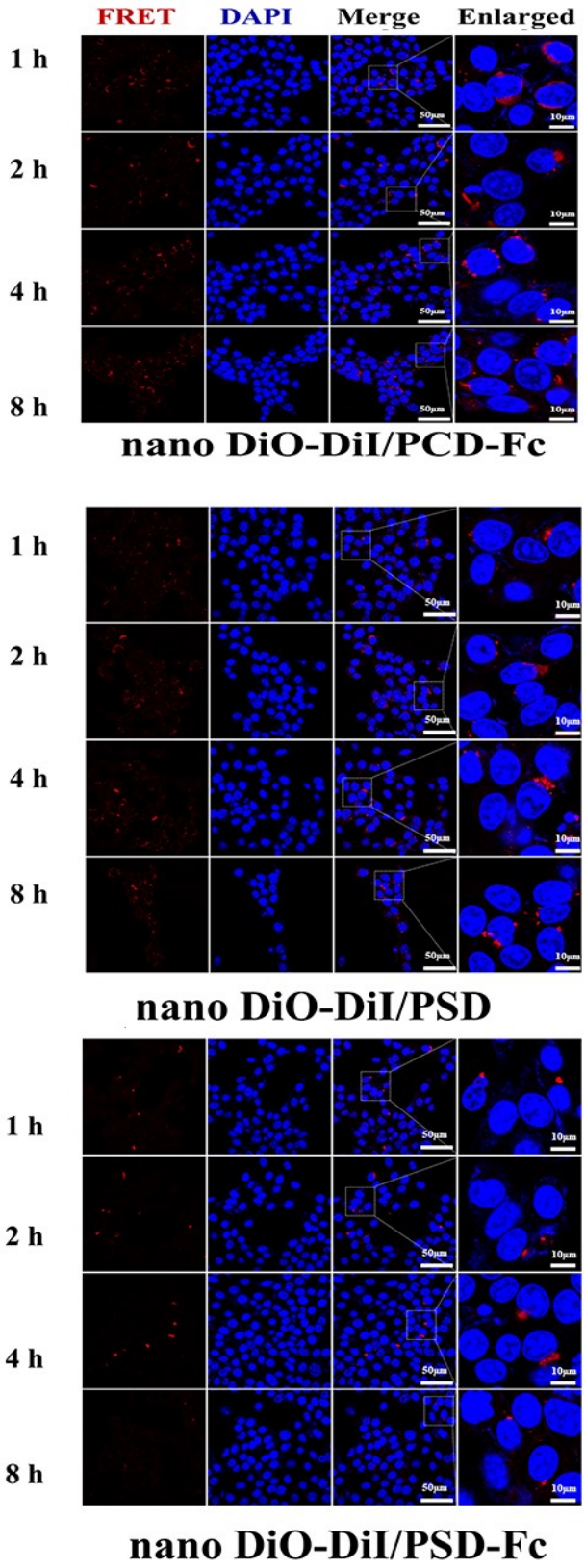

Figure S17. Time-dependent intracellular of nano DiO-DiI/PCD, nano DiO-DiI/PSD, and nano DiO-DiI/PSD-Fc in 4T1cells imaged by CLSM.

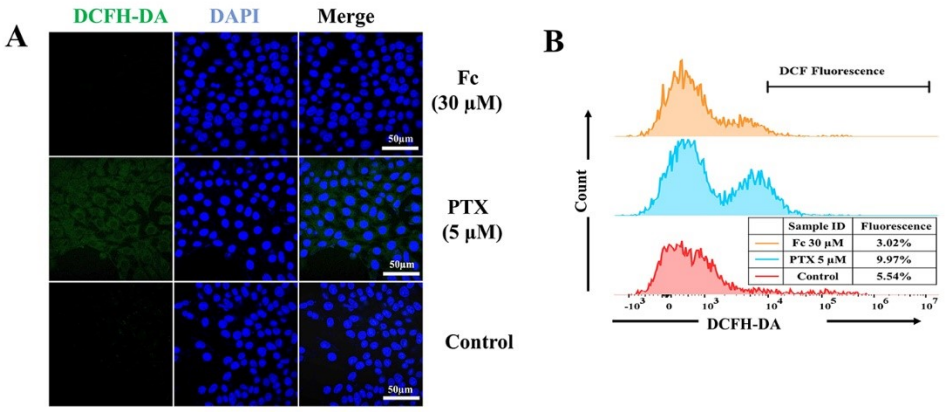

Figure S18. CLSM and flow cytometry images of the DCFH-DA probe in 4T1 cells after Fc, PTX treatments.

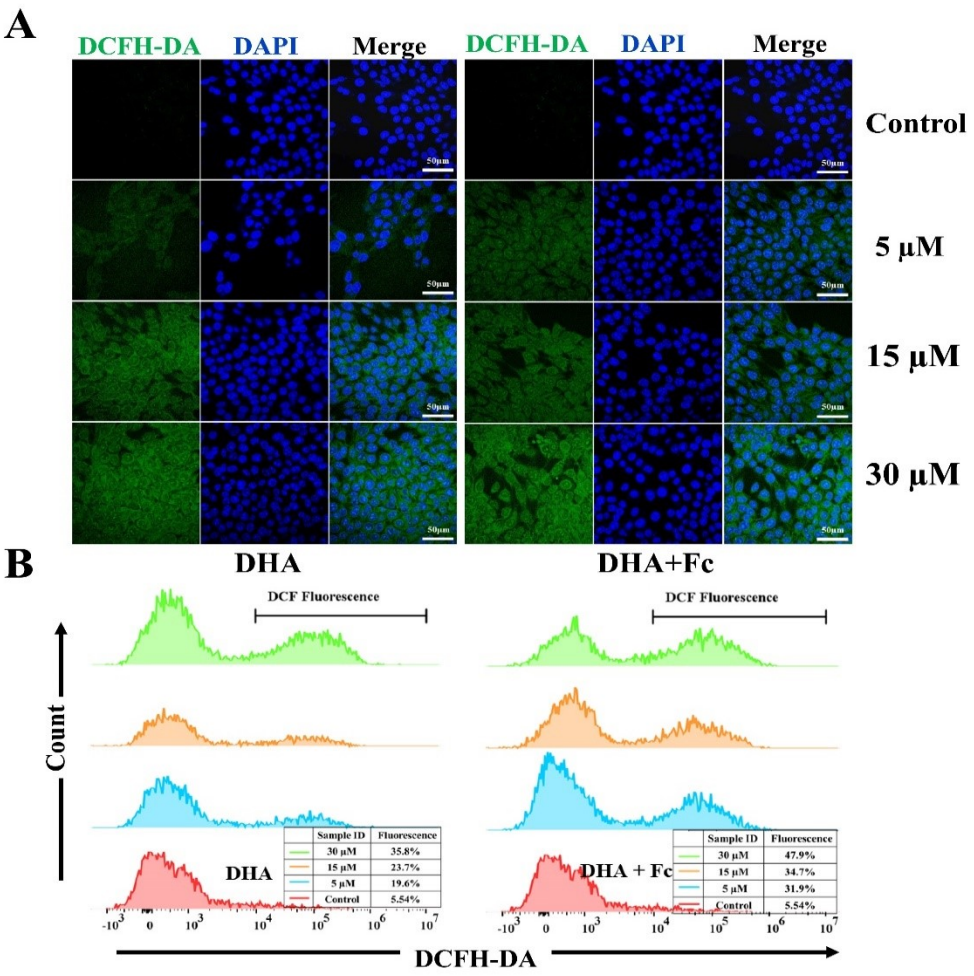

Figure S19. CLSM and flow cytometry images of the DCFH-DA probe in 4T1 cells after DHA, DHA+Fc treatments.

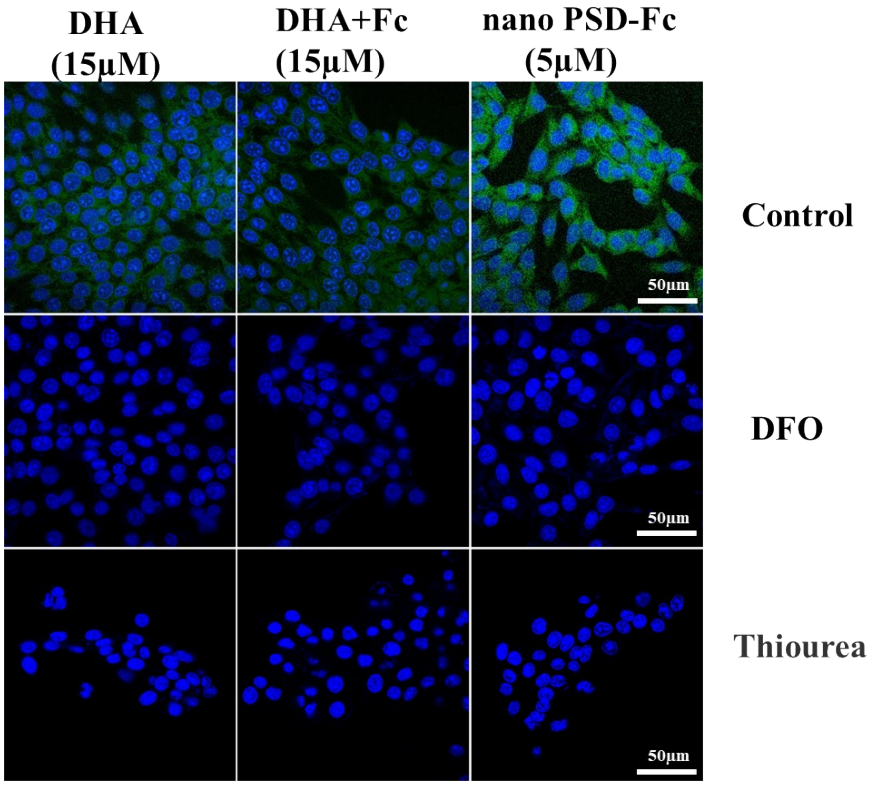

Figure S20. The CLSM image of the ROS generation in 4T1 cells after various treatments using the DCFH-DA probe with or without thiourea (ROS Scavenger), deferoxamine (DFO, iron chelation).

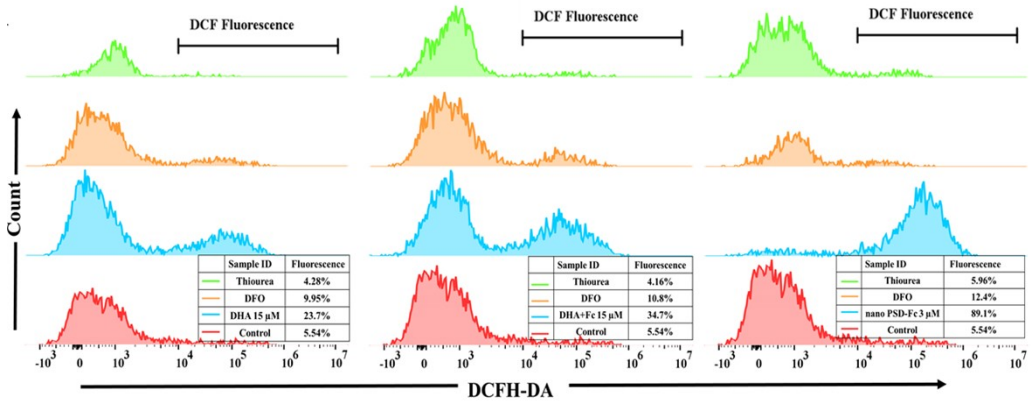

Figure 21.The flow cytometry analysis of the ROS generation in 4T1 cells after various treatments using the DCFH-DA probe with or without thiourea (ROS Scavenger), deferoxamine (DFO, iron chelation).

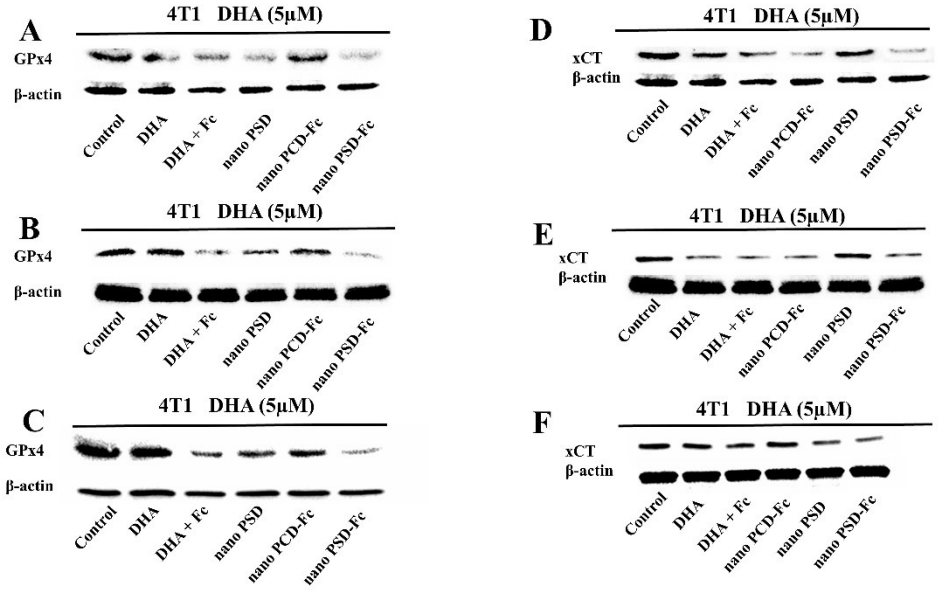

Figure S22. Western blot analysis of xCT and GPX4 after treatment with different formulations for 24h (DHA concentration at 5 μM)

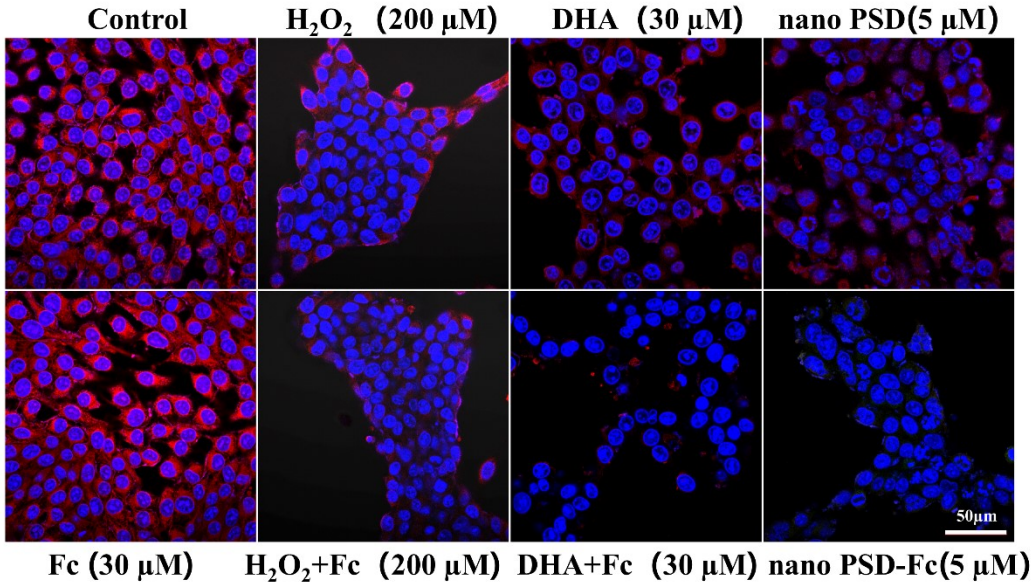

Figure S23. CLSM images of the BODIPY C11 probe in 4T1 cells after various treatments (ROS detection probe, 10 μM).

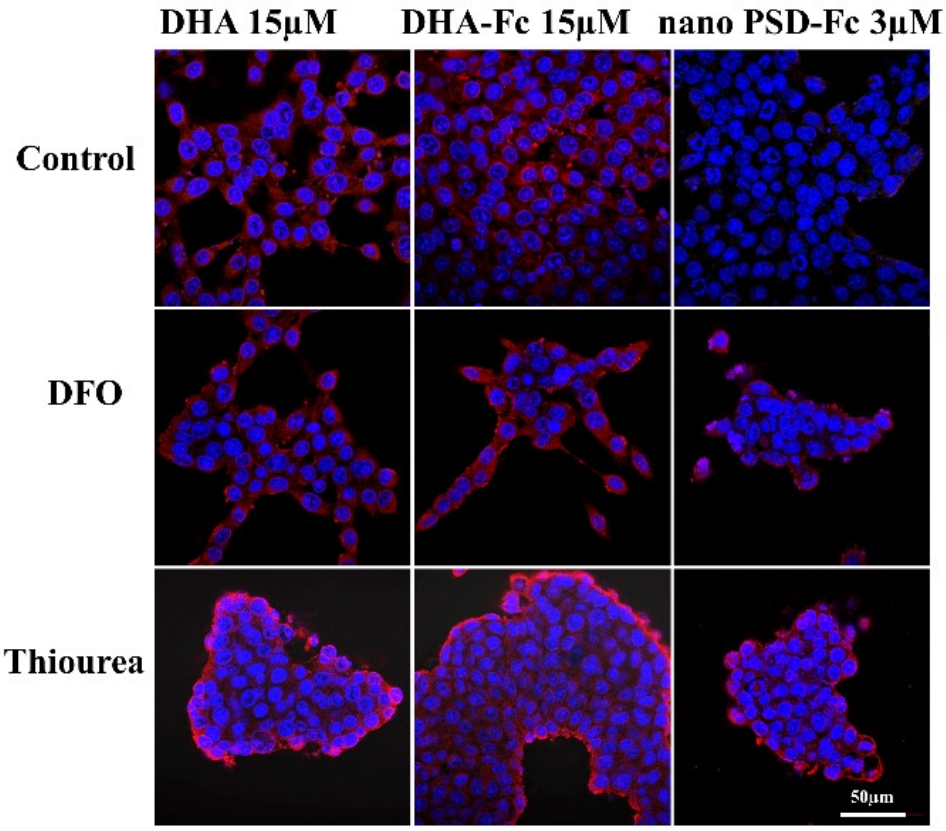

Figure S24. CLSM images of the BODIPY C11 probe in 4T1 cells after various treatments with or without thiourea (ROS Scavenger), deferoxamine (DFO, iron chelation).

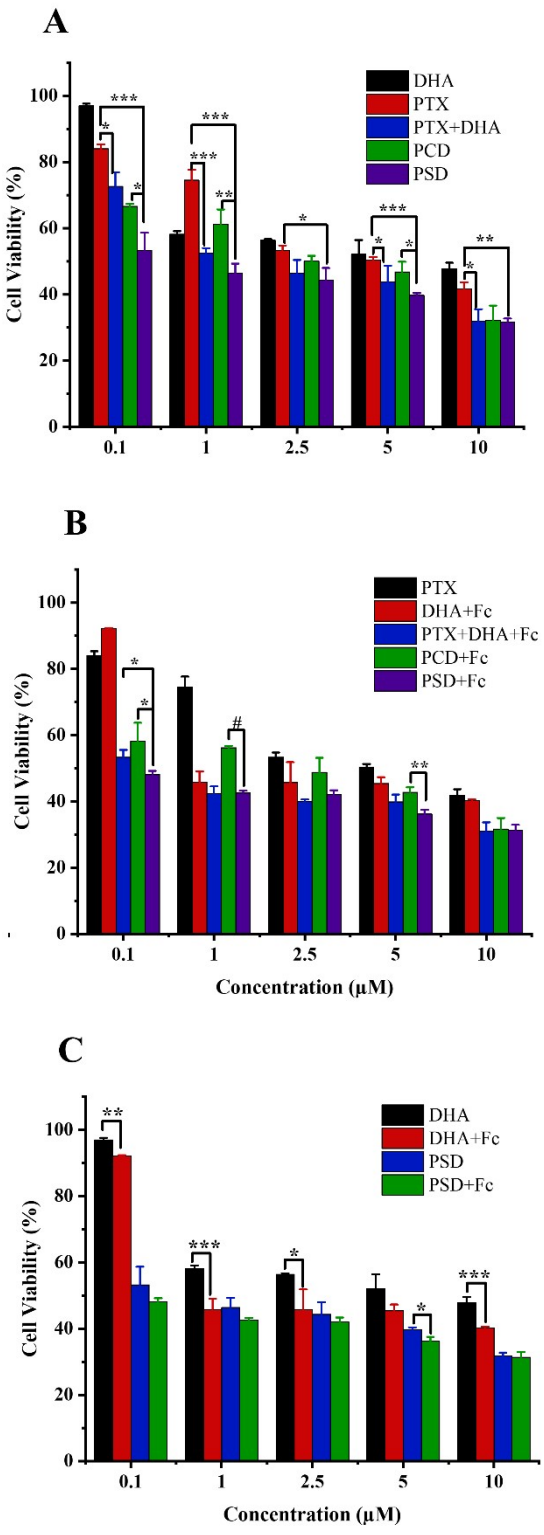

Figure S25. *In vitro* cytotoxicity against 4T1 cell lines after being incubated with different free drugs for 24h.(data are mean±SD, n=3, $^{*}P\leqslant0.05$, $^{**}P\leqslant0.01$, $^{***}P\leqslant0.001$, $^{\#}P\leqslant0.0001$)

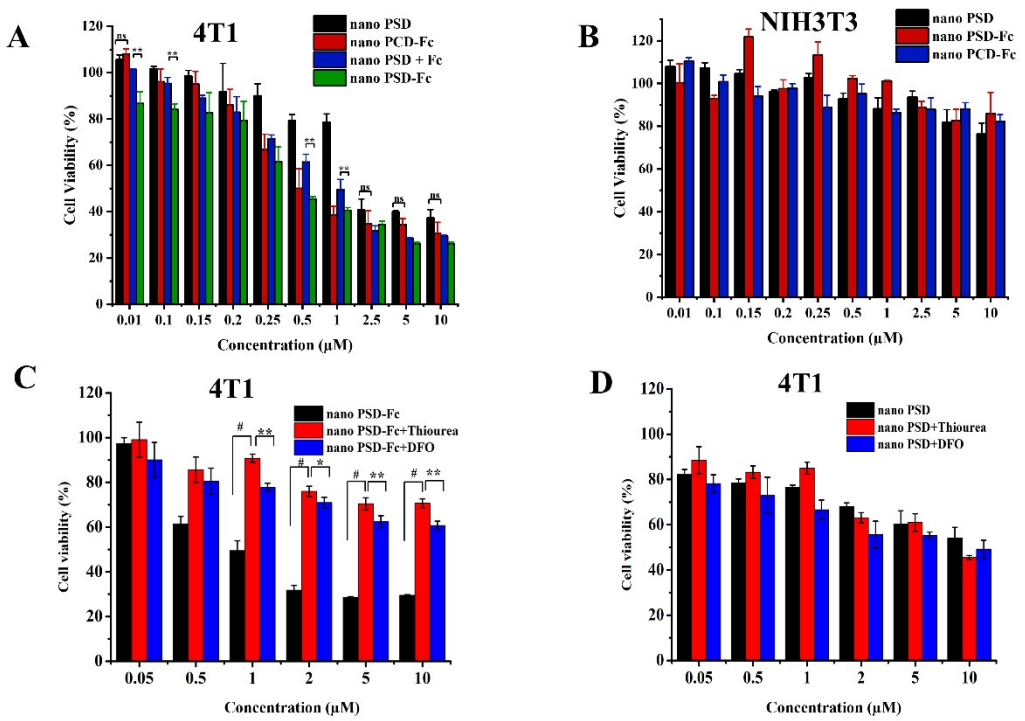

Figure S26. *In vitro* cytotoxicity against 4T1, NIH3T3 cell lines after being incubated with different formulations for 24h with or without thiourea (ROS Scavenger), deferoxamine (DFO, iron chelation).(data are mean±SD, n=3, $^{*}P\leqslant0.05$, $^{**}P\leqslant0.01$, $^{\#}P\leqslant0.0001$)

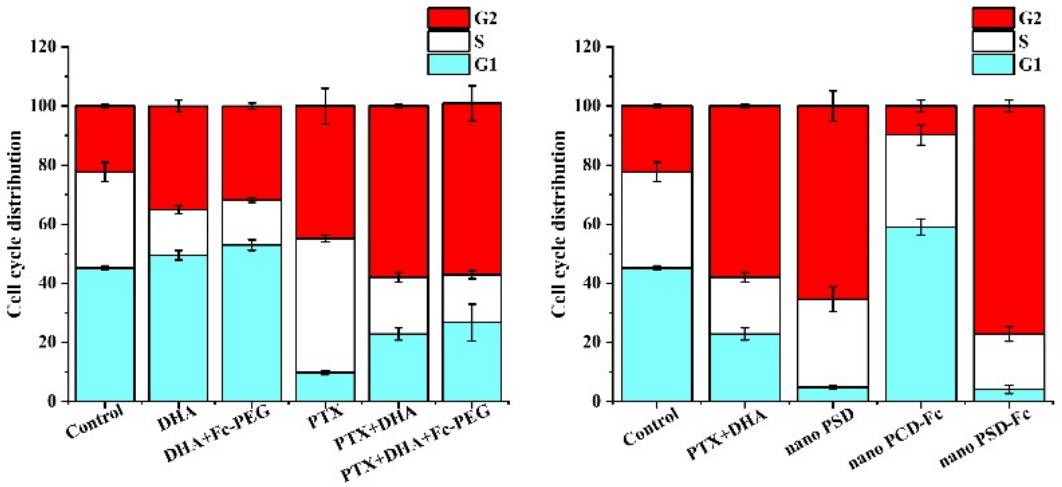

Figure S27. Flow cytometry analysis of cell cycle distribution in 4T1 cells after

treatment with different preparations. (data are mean±SD, n=3)

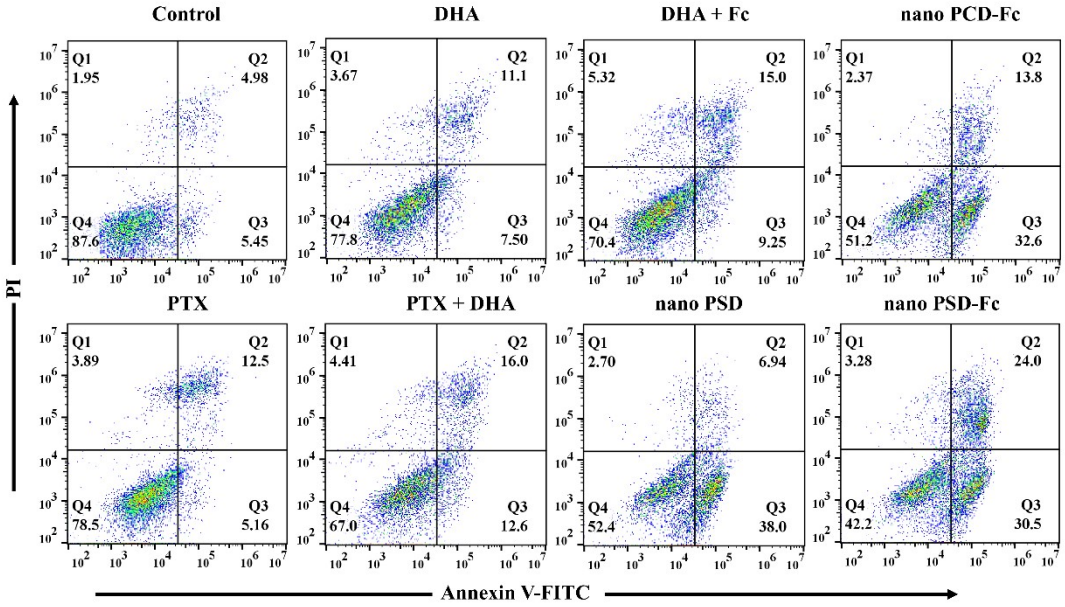

Figure S28. Flow cytometry analysis of apoptosis in 4T1 cells after treatment with different preparations.

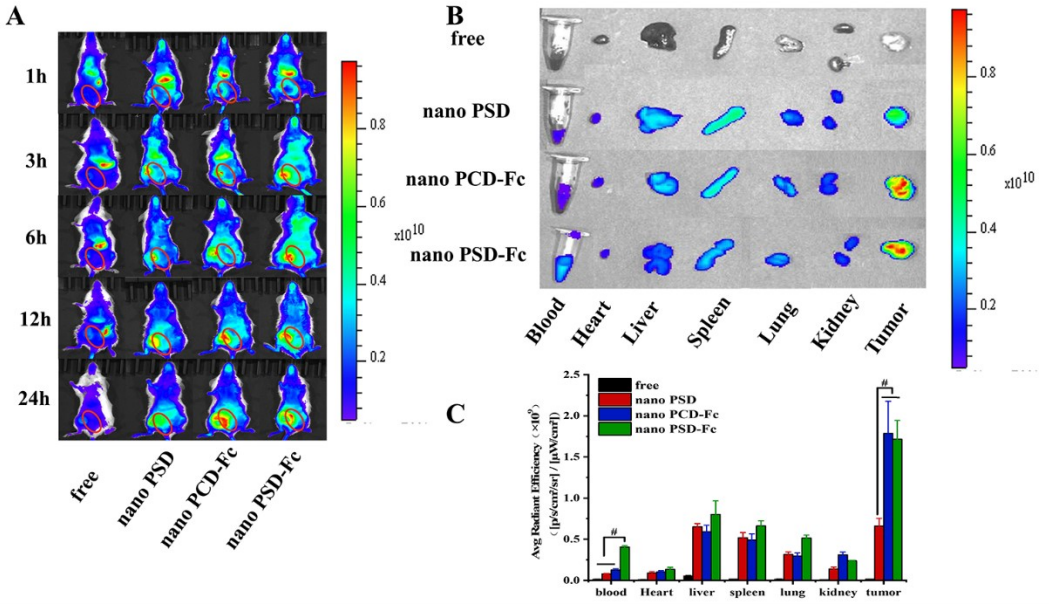

Figure S29. *In vivo* fluorescence images of the 4T1 bearing mice after intravenous

injection of DiR labeled nanoparticles (A), and Quantitative analysis of relative organ and tumor accumulation at 24 h (B-C). (data are mean ± SD, n=3, $^{\#}P \leqslant 0.0001$)

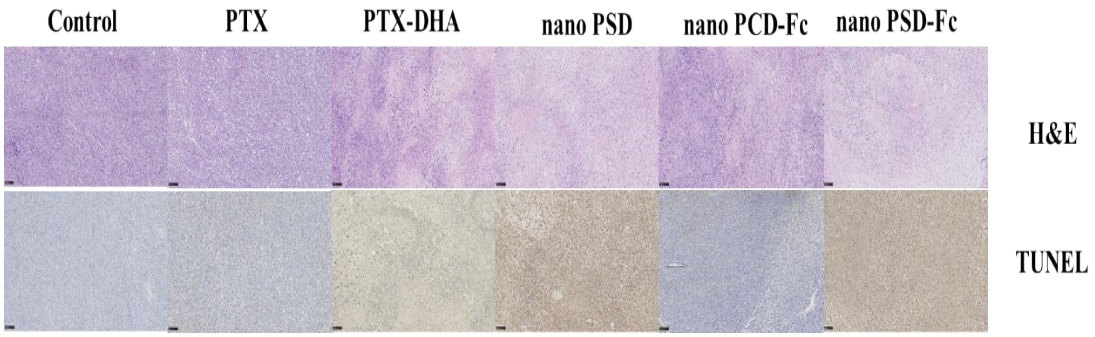

Figure S30. H&E and TUNEL images of 4T1 xenograft tumors after14-day treatments(bar=50 μm).

Table S1. Characterizations of the nanoparticles. (data are mean ± SD, n=3)

	nano PSD	nano PCD-Fc	nano PSD-Fc
Size (nm)	144.13±0.09	152.97±1.81	121.57±0.47
PDI	0.092±0.049	0.147±0.017	0.122±0.009
Zeta potential (mV)	-41.82±4.06	-34.32±2.37	-41.85±2.56
Loading efficiency	86.96 %	64.52 %	64.46 %